Title
Self-Assembly of Porphyrin-Containing Metalla-Assemblies and Cancer Photodynamic Therapy.

Journal
Inorganic Chemistry, 59(11)

Authors
Jiang, Xin
Zhou, Zhixuan
Yang, Huang
et al.

Publication Date
2020-06-01

DOI
10.1021/acs.inorgchem.9b02775

Peer reviewed

HHS Public Access

Author manuscript

Inorg Chem. Author manuscript; available in PMC 2021 June 01.

Published in final edited form as:

Inorg Chem. 2020 June 01; 59(11): 7380–7388. doi:10.1021/acs.inorgchem.9b02775.

Self-Assembly of Porphyrin-containing Metallacages and Cancer Photodynamic Therapy

Xin Jiang[†,§], **Zhixuan Zhou**[‡,§], **Huang Yang**[⊥], **Chuan Shan**[#], **Hao Yu**[†], **Lukasz Wojtas**[#], **Mingming Zhang**[‖], **Zhengwei Mao**[*,⊥], **Ming Wang**[*,†], **Peter J. Stang**[*,‡]

[†]Key Laboratory of Supramolecular Structure and Materials, College of Chemistry, Jilin University, Changchun, Jilin 130012, P. R. China

[‡]Department of Chemistry, University of Utah, 315 South 1400 East, Room 2020, Salt Lake City, Utah 84112, United States

[⊥]MOE Key Laboratory of Macromolecular Synthesis and Functionalization, Department of Polymer Science and Engineering, Zhejiang University, Hangzhou 310027, P. R. China

[#]Department of Chemistry, University of South Florida, 4202 East Fowler Avenue, Tampa, Florida 33620, United States

[‖]State Key Laboratory for Mechanical Behavior of Materials, Xi'an Jiaotong University, Xi'an 710049, P. R. China

Abstract

In this report, we describe the synthesis of two porphyrin-containing Pt (II) supramolecular cages via coordination-driven self-assembly. X-ray crystallographic analysis on one cage reveals that the metallacage formation imposes large interchromophore distances, leading to a higher $^1O_2$ generation efficiency relative to the corresponding small molecular precursors. The metallacages were examined as photosensitizers for photodynamic therapy as the potential reduction of the unfavorable self-aggregation phenomenon. *In vivo* and *in vitro* investigations demonstrate that the metallacages exhibit enhanced anticancer activity with minimal dose requirement and side effects comparable to the small molecule precursors. Thus, our work demonstrates that self-assembly provides a promising methodology for enhancing the therapeutic effectiveness of anti-cancer agents.

Graphical Abstract

[*]**Corresponding Author**: zwmao@zju.edu.cn (Z. M.), mingwang358@jlu.edu.cn (M. W.), stang@chem.utah.edu (P. J. S.).
[§]These authors contributed equally.

Author Contributions

The manuscript was written through contributions of all authors. All authors have given approval to the final version of the manuscript.

Supporting Information. The Supporting Information is available free of charge on the ACS Publications website at DOI: 10.1021/acs.inorgchem.9b02775. Electronic Supplementary Information (ESI) available: Synthetic and characterization data (NMR, ESI-MS, *in vitro* and *in vivo* experiment).

The authors declare no competing financial interest.

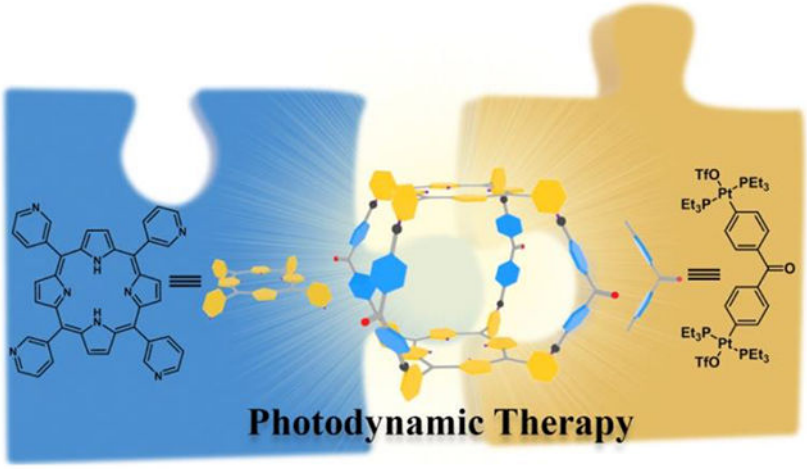

We designed and synthesized two metallacages via coordination-driven self-assembly between pyridyl-containing porphyrin motifs and a 120-degree di-Pt (II) motif. *In vitro and in vivo* experiments revealed that the metallacages efficiently inhibits the intramolecular and intermolecular stacking interactions of the porphyrin motifs and enhanced the effect of photodynamic therapy with a low dose and minimal side effects comparable to their small molecule precursors and cisplatin.

Introduction

Coordination-driven self-assembly is a powerful synthetic methodology for the preparation of discrete supramolecular coordination complexes (SCCs), including 2D metallacycles and 3D metallacages[1]. By the selection of electron-rich organic donors and electron-poor metal acceptors, SCCs with pre-designed, well-defined sizes and shapes can be obtained. As a result, the cavity size of the SCCs, as well as the distance and orientation of the functional groups incorporated within the SCCs, can be controlled, enabling precise functional modularity that lead to widespread applications in catalysis,[2] separation[3], and both light-emitting[4] and polymeric materials[5].

In the past few decades, photodynamic therapy (PDT) has been shown to be a promising clinical method for treating various types of cancer and infection[6]. PDT requires a combination of three elements: photosensitizer (PS), light, and molecular oxygen. Activation of PS by irradiation of a suitable wavelength of light leads to the formation of reactive oxygen species (ROS), which induce cell death[7]. Among the many PSs, porphyrin and its derivatives have attracted particular attention due to their favorable photophysical properties[6b,8]. However, porphyrin derivatives exhibit severe π-π stacking due to their large planar structures, which facilitate aggregation and thus reduce their ROS generation efficiency.[6b,7b,9] This characteristic has restrained the potential clinical applications of porphyrin derivatives and many other PSs. Although a lot of novel carrier systems have been developed to increase the solubility of porphyrin based PSs, reduce aggregation[10] and provide efficient transport direct to cancer cells,[11] it is still challenging to achieve molecular level of separation of PSs in these systems because of their strong molecular interactions.

Here, in order to regulate the aggregation of porphyrin-based PSs for improving anti-cancer performance, we design and synthesize two [2+4] metallacages, **1** and **2**, via the two-component coordination-driven self-assembly (Figure 1) between pyridyl-containing porphyrin motifs and a 120-degree di-Pt (II) motif. The two-component strategy provides structural simplicity and enhances stability compared to multi-component systems that explored previously,[8h] as shown by the NMR studies and electrospray ionization mass spectrometry (ESI-MS), which is favorable for studies in complicated biological systems. 3D coordination geometry of metallacage **1** was demonstrated by X-ray crystallographic analysis. The large, rigid structure of the metallacage has accurate component proportion and high structural stability. It can efficiently increase the distance of two porphyrin units and inhibits the aggregation caused by molecular interaction, contributing to obtain a higher ROS generation efficiency. *In vitro* and *in vivo* experiments were conducted to examine the anti-cancer activity of the metallacages, which revealed that both compounds exhibited potent anti-cancer activity with a low dose and minimal side effects. This work thus provides a promising methodology for efficient cancer treatment based on the design of supramolecular structures.

Results and discussion

Synthesis and Characterization of Metallo-Supramolecular Cages.

The metallacages were synthesized via the self-assembly of 5,10,15,20-tetra (3-pyridyl) porphine (**3**) or zinc 5,10,15,20-tetra(4-pyridyl)-21*H*,23*H*-porphine (**4**) with 120° diplatinium (II) motif (**5**) in a 1:2 stoichiometric ratio in DMSO at 80 °C for 12 h. The ^{1}H NMR of **1** and **2** both showed six sets of aromatic protons from the porphyrin units and the phenyl groups, which are consistent with the expected structures. All the protons corresponding to the pyridyl groups (H_{1a} to H_{1e}) exhibited downfield shifts upon the formation of **1** due to the loss of electron density upon coordination with platinum metal centers, while the peak corresponding to the pyrrole H_{1f} shifted upfield (Figure 2a–e). This phenomenon is also manifested in the ^{1}H NMR spectra of **2** and its ligand **4**. The ^{31}P{^{1}H} NMR spectra of 1 and 2 both display a singlet with concomitant 195Pt satellites (δ = 12.64 ppm for 1 and 12.73 ppm for 2, respectively) (Figure 2f–h), which was shifted upfield relative to the acceptor 5 (δ = 18.99 ppm), due to the electron back-donation from the platinum atoms. The signals in the ^{31}P{^{1}H} NMR, ^{1}H NMR, and 2D COSY NMR (Figures S3–12) spectra illustrate the formation of discrete and highly symmetric metallacages.

Electrospray ionization mass spectrometry (ESI-MS) provides evidence for the formation of the metallacages. A series of peaks with different charge states from 3+ to 6+ were observed for both **1** and **2** due to the loss of the triflate (OTf^{-}) counterions. The isotope patterns of these peaks are in good agreement with the theoretical simulations (Figures 2i, j and Figure S1–2). After deconvolution of *m/z*, the molecular weights for **1** and **2** were determined to be 6600 and 6732 Da, respectively, confirming that these complexes are composed of two **3** or **4** and four diplatinum (II) acceptors **5**.

Single crystals of **1** were obtained by slow vapor diffusion of diethyl ether into a nitromethane solution of the cage (OTf^{-} salt) over four weeks. In the solid state,

1•4OTf•solv crystallizes in monoclinic space group P2/c with a slight positional disorder, due to the flexible nature of the pyridyl groups in **3**. The cage consists of two parallel porphyrins linked by four di-Pt (II) motifs. The di-Pt (II) motif adopts an angle of 125°, likely due to the slight twisting of the porphyrin group. The distance between the parallel Pt (II) building blocks is 23.4 Å, while the distance between the two porphyrin panels was found to be 18.3 Å (Figure 2k). The formations of ordered and complementary crystal arrangements are provided in Supporting Information (Figure S13 and Table S1). As such, the metallacage formation via coordination efficiently separates the porphyrin groups, prohibiting the tight packing that is undesirable for practical applications.

Photophysical Properties.

The UV-vis absorption spectra of **1** and **2** were recorded in DMSO (Figure 3a). Several absorption wavelengths were observed in Q band from 450 to 650 nm, which was attributed to the absorption transition between the ground state and the first excited singlet state (S0 - S1). A broad absorption band centered at 638 nm was observed in **1**. The chelation of Zn ion in **2** led to hypsochromically-shifted Q-bands compared with **1**[12]. This indicates that **1** has more advantages over **2** in practical biological experiments owing to its stronger penetrating ability on account of the redder absorption wavelength.

Fabrication of Supramolecular Cage Loaded Nanoparticles.

Since **1** and **2** are hydrophobic and not well dispersed in the aqueous media, amphiphilic block polymer PEBP-b-PEG-cRGD (Figures 3b and Fig. S14) was used to encapsulate them into the core of hydrophilic nanoparticles (denoted as **1 NPs** and **2 NPs**, respectively) to enhance their colloidal stability and circulation time for further *in vivo* applications[13]. Furthermore, the accumulation of nanoparticles in tumors can be expected with the collective effects based on the enhanced permeability and retention (EPR) effect and active targeting ability of cRGD moieties[14].

The morphologies and sizes of the nanoparticles were investigated by transmission electron microscopy (TEM) and dynamic laser scattering (DLS). Spherical **1 NPs** with diameters ranging from 30 to 90 nm were observed in the TEM study (Figure S15A). A slightly larger hydrophilic diameter was recorded from DLS (Figure S15B) due to the hydration of the NPs. An enhancement in diameter from 35.7 to 61.8 nm was observed after loading **1** into the nanoparticles, indicating the successful encapsulation of the cages by the amphiphilic polymers. Furthermore, the zeta potential of the nanoparticles increased from −46.9 mV to −5.4 mV upon encapsulation of 1 (Figure S15C), suggesting that the electrostatic interaction is one of the major driving forces in the formation of self-assemblies, in addition to hydrophobic interaction. The **1 NPs** are stable in phosphate-buffered saline (PBS) containing 10% fetal bovine serum at 37 °C over 48 h of incubation (Table S2), demonstrating promising colloidal stability of **1 NPs** in biological milieus.

Singlet oxygen sensor green (SOSG) was used to quantify the reactive oxygen species (ROS) generation of the nanomaterials upon laser irradiation (638 nm, 0.5 W/cm^2). We used the same molar concentration of porphyrin units (500 nM) to compare the ROS production ability between metallacage and porphyrin alone. As shown in Figure 3c, low fluorescence

enhancement was observed from **3** and **3**-cored nanoparticles (**3 NPs**) due to the poor ROS generation efficiency induced by strong π-π stacking interactions. In contrast, a 4-fold enhancement for the SOSG fluorescence is observed upon the introduction of cage structure (**1 NPs**), suggesting a high photosensitizing efficacy. The high yield of ROS generation from **1 NPs** can be attributed to the supramolecular cage structure to efficiently prevent the aggregation of porphyrin units and the incorporation of platinum atoms in the cage. This is beneficial for the generation of reactive singlet oxygen species by promoting intersystem crossing[15]. Compared to **1 NPs**, incorporation of Zn ions in **2 NPs** leads to lower ROS generation efficiency under laser irradiation due to the hypsochromically-shifted Q-bands (Figure 3d).

In Vitro Cytotoxicity.

The presence of cRGD within **1 NPs** should endow the nanoparticle with tumor targeting capability[16]. Receptor-mediated uptake of the **1 NPs** in mouse triple-negative breast cancer cells (4T1) was quantitatively confirmed by flow cytometry and inductively coupled plasma mass spectrometry (ICP-MS) (Figure 4a and b). Faster and higher cellular internalization of **1 NPs** is observed relative to the nanoparticles without cRGD modification.

The cytotoxicity of the compounds in the dark and subjected light irradiation (+Light) was quantified using 3-(4',5'-dimethylthiazol-2'-yl)-2,5-diphenyl tetrazolium bromide (MTT) assay (Figure 4c and Table S3). The Pt (II) acceptor displayed moderate cytotoxicity, with half-maximal inhibitory concentration in dark (IC_{50}) values of 7.85 ± 0.8 μM and 8.15 ± 0.7 μM for **5** and **5** + Light, respectively. These values are higher than that of commercially available cisplatin (IC_{50} = 4.39 ± 0.7μM). This result also suggests that light irradiation on 5 cannot enhance its toxicity. In contrast, **3 NPs** did not show obvious cytotoxicity without laser irradiation, while the half-maximal inhibitory concentration with light irradiation (LD_{50}) of **3 NPs** was determined to be 0.51 ± 0.12 μM upon light irradiation (638 nm for 2 min, 0.2 W/cm^2). The most encouraging results were observed from the **1 NPs** + Light group, showing an LD_{50} value of 0.087 ± 0.009 μM upon irradiation, which was much lower than those of the small molecular precursors. From our previous study, we found the SCCs can interact with DNA due to the binding effect between Pt and DNA bases.[4h] It is possible that the cages degrade in biological environment and release out Pt fragment and show anti-cancer actions. The phototoxicity index (PTI) which defines the ratio of the IC_{50} in the dark and LD_{50} under light irradiation was calculated to be 40.7. It is quite difficult to directly compare the PDT performance based on PTI because the lasers are different. At least the PTI of **1 NPs** is comparable to aminolaevulinic acid (ALA), which is the porphyrin prodrug used in clinic.[17] The results suggested the potential of the **1 NPs** as an efficient PS for PDT treatment. Annexin V-FITC/PI assay (Figure S16) and fluorescence in diacetate/propidium iodide (FDA/PI) co-staining assay (Figure S17) also suggest that **1 NPs** possesses potent PDT effect.

In Vivo Distribution.

In order to study their pharmacokinetics, the **1 NPs** and free **5** were intravenously (i.v.) injected into the mice at a dose of 2 mg/kg platinum. Blood samples were collected at various time points after injection. By quantifying the blood platinum concentration using

ICP-MS, the blood circulation half-life of the **1 NPs** was calculated to be 2.39 ± 0.4 h, 4.5 times that of **5** (Figure 5a). Approximately 11.4% **1 NPs** of the injected dose (ID) remained in the plasma at 24 h. While **5** was almost completely eliminated from the bloodstream 8 h post injection.

The area under the curve (AUC) of the **1 NPs** significantly increased to 149 μg mL^{-1} h, 18.9-fold higher than that of **5** (7.86 μg mL^{-1} h). These results suggest that **1 NPs** possess a size favorable for long circulation and selective accumulation in the tumor site, which may lead to improved therapeutic efficacy and reduced side effects. Prolonged circulation of nanoparticles in the bloodstream is indispensable for successful targeted delivery and efficient treatment, which was achieved by surface-grafting of PEG shells, thereby preventing them from being cleared by the reticuloendothelial system (RES)[18].

To acquire a quantitative assessment of the bio-distribution profile of the **1 NPs**, the platinum contents of different organs were analyzed by ICP-MS (Figure 5b). Bio-distribution evaluations indicated that the **1 NPs** effectively accumulated in the tumor, approaching 2.24 ± 0.31 μg/g tissue **24** h post administration, which was significantly higher than that of 5 (0.39 ± 0.05 μg/g tissue, Figure S18). A high concentration of **1 NPs** can be observed in the liver, which was attributed to the RES capture and subsequent excretion. Precursor **5** showed a significantly different distribution in major organs compared to that of **1 NPs**, mainly located at the kidney. These findings suggest that **1 NPs** were more widely available for tumor uptake than small molecular drugs, while also reducing the adverse effects towards normal tissues.

In Vivo PDT.

In vivo antitumor efficacy of the **1 NPs** was evaluated on the highly aggressive 4T1 orthotopic breast cancer-bearing mice. 4T1 orthotopic tumor-bearing mice with tumor volume around 130 mm^3 were randomly divided into six groups, and administered with physiological saline, cisplatin, **5, 3 NPs** + Light, **1 NPs**, and **1 NPs** + Light, respectively. A laser with low power density (0.5 W/cm^2) and optimized irradiation time (6 min) was chosen for PDT at 24 h post i.v. injection. No noticeable skin burning was observed by application of the laser alone. The tumors of the mice administered with saline grew rapidly (Figure 5c), exhibiting a 13.0-fold increase of tumor volumes after 21 days as compared with their original volume. The growth of tumors was slightly reduced by cisplatin, **5** or **1 NPs**. Although the tumor size was notably reduced by the PDT in the first 6 days for the group subjected to **3 NPs** + Light, a rapid recovery of tumor growth was evident afterwards, likely due to the relatively low ROS generation of **3 NPs** that was unable to clear all cancer cells distal from the primary tumor. **1 NPs** + Light displayed the highest anti-tumor efficacy among these groups and almost completely eradicated tumors without recurrence (5 out of 6 mice) in the experimental period. The tumors were excised after 21 days post-treatment, and the weights of the tumors were assessed (Figures 5d and S19). The tumor growth inhibition ratio of the groups treated with **1 NPs** upon light irradiation was 98.4%, while those for **1 NPs, 5, 3 NPs** + Light, and cisplatin was 51.5%, 37.3%, 60.5%, and 31.2%, respectively. These results demonstrated the anti-tumor efficacy of **1** by laser-irradiation-activated PDT to ablate the tumor without recurrence after a single treatment.

Immunohistochemical analyses were supportive of the results concerning tumor inhibition discussed above (Figure 5e). Hematoxylin and eosin (H&E) stain revealed that tumors in the control groups showed varying levels of recession compared with the saline-treated group. For the mice treated with **1 NPs** + Light, no tumor cells were observed, suggesting successful destruction of the tumor. Ki67-positive immunohistochemical staining further revealed the lowest proliferation (brown spots) in the tumor area from the photo-chemotherapy group (**1 NPs**+ Light).

The systemic toxicity of the nanomedicine was evaluated using body weight loss and survival rate as indications. For **5** and cisplatin administrations, the body weight of mice decreased within the first week due to their systematic toxicity and related side effects (Figure 5g). Histological analyses provided insight into the systemic toxicity caused by **5** or cisplatin. Some pulmonary and hepatic damage was observed from the mice in **5** in cisplatin groups (Figures S20–21). In contrast, no apparent changes in body weight and histological examination were observed from the mice receiving other treatments (Figures S22–24), implying that **1 NPs** + Light has minimal systemic toxicity to mice after a single injection. The median survival rates for the mice treated with saline, **1 NPs, 5, 3 NPs** + Light, and cisplatin were calculated to be 36, 49, 42, 54, and 42 d, respectively; whereas PDT using **1 NPs** + Light greatly prolonged mice survival over 75 days with a single death (Figure 5f). These results demonstrated PDT using **1 NPs** + Light effectively prolonged mice lifespans without obvious side effects. A positive therapeutic effect was also observed on the cisplatin-resistant tumor model *in vitro* and *in vivo* (Figures S25–26).

The lung tissues were collected and investigated after the mice were sacrificed (Figure S27A) to study the anti-metastatic effect of **1 NPs**. The average metastatic tumor nodules per lung were counted to be 5.67, 2.17, 3.67, 1.17, and 4.2 for the mice treated with saline, **1 NPs, 5, 3 NPs** + Light, and cisplatin, respectively (Figure S27B). The tumor coverage percentages of the lung surface were calculated to be 9.33%, 2.23%, 4.37%, 0.83%, and 5.51% for the mice treated with saline, **1 NPs, 5, 3 NPs** + Light, and cisplatin, respectively (Figure S27C). In contrast to these groups, only one tumor nodule was visualized from the six lungs of mice that received the combinational treatment using **1 NPs** + Light. The average tumor coverage on the lung surface was only 0.07%, indicating strong anti-metastatic efficacy of the PDT by **1 NPs**.

Conclusions

In summary, we designed and synthesized two supramolecular metallacages using the coordination-driven self-assembly between porphyrin derivatives (**3** and **4**) and 120° bimetallic Pt (II) acceptors (**5**). The single crystal of **1** indicates that the formation of metallacages efficiently inhibits the intramolecular and intermolecular stacking interactions of the porphyrin motifs, leading to a higher ROS generation efficiency relative to the precursor. **1 NPs** and **2 NPs** were prepared by encapsulating the metallacages into the core of hydrophilic nanoparticles by using amphiphilic block polymer PEBP-b-PEG-cRGD, which enhances their colloidal stability and prolongs their circulation time. **1 NPs** showed an IC_{50} value of 0.087 ± 0.009 μM upon light irradiation, which was significantly lower than those of the small molecule precursors. *In vivo* studies suggest that PDT **1 NPs** exert tumor

inhibition effects without recurrence and metastasis after a single treatment against orthotopic breast cancers and drug-resistant cancers. This research provides a promising strategy for efficient cancer treatment by modulating the properties of functional motifs using self-assembly.

Experimental section

General Procedures.

Compound **5**,[19] **4**[20] and **PEBP-b-PEG-cRGD**[13c,11c] were prepared according the reported literature. All reagents were purchased from Sigma-Aldrich, Matrix Scientific, Alfa Aesar and used without further purification. Column chromatography was conducted using basic Al_2O_3 (Brockman I, activity, 58 Å) or SiO_2 (VWR, 40-60 μm, 60 Å) and the separated products were visualized by UV light. NMR spectra data were recorded on a 500-MHz Bruker Avance NMR spectrometer in $CDCl_3$, DMSO-d_6 with TMS as reference. ESI-MS was recorded with a Waters Synapt G2 tandem mass spectrometer, using solutions of 0.5 mg sample in 1 mL of DMSO/MeOH/Acetone (1:1:3, v/v) for complexes. The X-ray diffraction data were measured on Bruker D8 Venture PHOTON II CPAD system equipped with a Cu Kα INCOATEC ImuS micro-focus source (λ = 1.54178 Å). The TEM images of the drop cast samples were taken with a JEOL 2010 transmission electron microscope.

Synthesis of Complex 1: 3 (10.0 mg, 16.2 μmol) and **5** (43.4 mg, 32.4 μmol) were weighed accurately and dissolved in 2.5 mL DMSO, and the mixture was heated at 80 °C for 10 h. After cooling to room temperature, excessive amount of diethyl ether was added and a precipitate was formed, which was filtered and washed with diethyl ether, then dried in vacuo to get a dark brown solid (51.5mg, 96.4%). ^{1}H NMR (500 MHz, DMSO-d_6, 300 K, ppm) :δ 9.60 (m, 8H, Py-H^a), δ 9.33 (d, 8H, Py-H^b), δ 8.94 (m, 24H, Py-H^d, P-H^e), δ 8.28 (t, 8H, Py-H^c), δ 7.63 (d, 16H, Ph-H^2), δ 7.20-7.30 (m, 16H, Ph-H^1), δ −3.13 (s, 4H, P-H^f). ^{13}C DEPTQ NMR (500 MHz, DMSO-d_6, 300 K, ppm) δ 194.01, 154.46, 153.24, 143.76, 142.94, 140.53, 137.29, 135.39, 131.93, 130.08, 128.92, 127.06, 122.01, 119.86, 115.42, 42.57, 41.80, 40.89, 12.65, 7.89. ESI-MS (*m/z*): 2049.2 $[M\text{-}3OTf^-]^{3+}$ (calcd m/z: 2049.2), 1500.9 $[M\text{-}4OTf^-]^{4+}$ (calcd m/z: 1500.9), 1170.7 $[M\text{-}5OTf^-]^{5+}$ (calcd m/z: 1170.7), 950.6 $[M\text{-}6OTf^-]^{6+}$ (calcd m/z: 950.6).

Synthesis of Complex 2: 4 (10 mg, 14.7 μmol) and **5** (39.4 mg, 29.4 μmol) were weighed accurately and dissolved in 2.5 mL DMSO, and the mixture was heated at 80 °C for 10 h. After cooling to room temperature, excessive amount of diethyl ether was added and a precipitate was formed, which was filtered and washed with diethyl ether, then dried in vacuo to get a dark purple solid (47.0 mg, 95.1%). ^{1}H NMR (500 MHz, DMSO-d_6, 300 K, ppm): δ 9.60 (s, 8H, Py-H^a), δ 9.29-9.30 (d, 8H, Py-H^b), δ 8.84-8.87 (m, 24H, Py-H^d, ZP-H^e), δ 8.22-8.25 (t, 8H, Py-H^c), δ 7.64 (d, 16H, Ph-H^2), δ 7.21-7.32 (m, 16H, Ph-H^1). ^{13}C DEPTQ NMR (500 MHz, DMSO-d_6, 300 K, ppm) δ 193.98, 154.08, 152.81, 150.01, 143.60, 142.80, 141.78, 137.27, 135.40, 132.49, 131.92, 130.10, 128.90, 126.72, 122.27, 119.71, 115.53, 41.81, 12.64, 7.88. ESI-MS (*m/z*): 2093.2 $[M\text{-}3OTf^-]^{3+}$ (calcd m/z: 2093.2), 1532.4 $[M\text{-}4OTf^-]^{4+}$ (calcd m/z: 1532.4), 1196.1 $[M\text{-}5OTf^-]^{5+}$ (calcd m/z: 1196.1), 971.8 $[M\text{-}6OTf^-]^{6+}$ (calcd m/z: 971.8).

Supplementary Material

Refer to Web version on PubMed Central for supplementary material.

ACKNOWLEDGMENT

This work was supported by the Program for JLU Science and Technology Innovative Research Team and Natural Science Foundation of Jilin Province (20180101297JC), National Natural Science Foundation of China (51822306) and the National Key R&D Program of China (2016YFE0132700). P. J. S. thanks NIH (Grant R01 CA215157) for financial support.

REFERENCES

(1). (a)Chakrabarty R; Mukherjee PS; Stang PJ Supramolecular Coordination: Self-Assembly of Finite Two- and Three-Dimensional Ensembles. Chem. Rev 2011, 111, 6810; [PubMed: 21863792] (b)Faiz JA; Heitz V; Sauvage J-P Design and Synthesis of Porphyrin-containing Catenanes and Rotaxanes. Chem. Soc. Rev 2009, 38, 422; [PubMed: 19169458] (c)Chakraborty S; Newkome GR Terpyridine-based Metallosupramolecular Constructs: Tailored Monomers to Precise 2D-motifs and 3D-metallocages. Chem. Soc. Rev 2018, 47, 3991; [PubMed: 29594272] (d)Fujita M; Tominaga M; Hori A; Therrien B Coordination Assemblies from a Pd(II)-Cornered Square Complex. Acc. Chem. Res 2005, 38, 369; [PubMed: 15835883] (e)Sepehrpour H; Fu W; Sun Y; Stang PJ Biomedically Relevant Self-Assembled Metallacycles and Metallacages. J. Am. Chem. Soc, 2019, 141, 14005. [PubMed: 31419112] (f)Clever GH; Punt P Cation-Anion Arrangement Patterns in Self-Assembled Pd_2L_4 and Pd_4L_8 Coordination Cages. Acc. Chem. Res 2017, 50, 2233; [PubMed: 28817257] (g)Zheng YR; Zhao ZG; Wang M; Ghosh K; Pollock JB; Cook TR; Stang PJ A Facile Approach Toward Multicomponent Supramolecular Structures: Selective Self-Assembly via Charge Separation. J. Am. Chem. Soc 2010, 132, 16873; [PubMed: 21053935] (h)Bhat IA; Samanta D; Mukherjee PS A Pd_{24} Pregnant Molecular Nanoball: Self-Templated Stellation by Precise Mapping of Coordination Sites. J. Am. Chem. Soc 2015, 137, 9497; [PubMed: 26161983] (i)Rizzuto FJ; Ramsay WJ; Nitschke JR Otherwise Unstable Structures Self-Assemble in the Cavities of Cuboctahedral Coordination Cages. J. Am. Chem. Soc 2018, 140, 11502; [PubMed: 30114908] (j)Cremers J; Richert S; Kondratuk DV; Claridge TDW; Timmel CR; Anderson HL Nanorings with Copper(ii) and Zinc(ii) Centers: Forcing Copper Porphyrins to Bind Axial Ligands in Heterometallated Oligomers. Chem. Sci 2016, 7, 6961; [PubMed: 28451130] (k)Wang C; Hao X-Q; Wang M; Guo C; Xu B; Tan EN; Zhang Y-Y; Yu Y; Li Z-Y; Yang H-B; Song M-P; Li X Self-Assembly of Giant Supramolecular Cubes with Terpyridine Ligands as Vertices and Metals on Edges. Chem. Sci 2014, 5, 1221;(l)Percástegui EG; Mosquera J; Ronson TK; Plajer AJ; Kieffer M; Nitschke JR Waterproof Architectures through Subcomponent Self-Assembly. Chem. Sci 2019, 10, 2006; [PubMed: 30881630] (m)Shanmugaraju S; Jadhav H; Patil YP; Mukheijee PS Self-Assembly of an Octanuclear Platinum(II) Tetragonal Prism from a New Pt^{II}_4 Organometallic Star-Shaped Acceptor and Its Nitroaromatic Sensing Study. Inorg. Chem 2012, 51, 13072; [PubMed: 23181445] (n)Ghosh S; Mukherjee PS Self-Assembly of Molecular Nanoball: Design, Synthesis, and Characterization. J. Org. Chem 2006, 71, 8412; [PubMed: 17064013] (o)Saha ML; Schmittel M Degree of Molecular Self-Sorting in Multicomponent Systems. Org. Biomol. Chem 2012, 10, 4651. [PubMed: 22543924]

(2). Ueda Y; Ito H; Fujita D; Fujita M Permeable Self-Assembled Molecular Containers for Catalyst Isolation Enabling Two-Step Cascade Reactions. J. Am. Chem. Soc 2017, 139, 6090. [PubMed: 28402111]

(3). Shi Y; Cai K; Xiao H; Liu Z; Zhou J; Shen D; Qiu Y; Guo Q-H; Stern C; Wasielewski MR; Diederich F; Goddard WA; Stoddart JF Selective Extraction of C_{70} by a Tetragonal Prismatic Porphyrin Cage. J. Am. Chem. Soc 2018, 140, 13835. [PubMed: 30265801]

(4). Zhang M; Yin S; Zhang J; Zhou Z; Saha ML; Lu C; Stang PJ Metallacycle-Cored Supramolecular Assemblies with Tunable Fluorescence including White-Light Emission. Proc. Natl. Acad. Sci. U. S. A 2017, 114, 3044. [PubMed: 28265080]

(5). (a)Gu Y; Alt EA; Wang H; Li X; Willard AP; Johnson JA Photoswitching Topology in Polymer Networks with Metal–Organic Cages as Crosslinks. Nature 2018, 560, 65. [PubMed: 30022167] (b)Zheng W; Chen L-J; Yang G; Sun B; Wang X; Jiang B; Yin G-Q; Zhang L; Li X; Liu M; Chen G; Yang H-B Construction of Smart Supramolecular Polymeric Hydrogels Cross-linked by Discrete Organoplatinum(II) Metallacycles via Post-Assembly Polymerization. J. Am. Chem. Soc 2016, 138, 4927. [PubMed: 27011050]

(6). (a)Celli JP; Spring BQ; Rizvi I; Evans CL; Samkoe KS; Verma S; Pogue BW; Hasan T Imaging and Photodynamic Therapy: Mechanisms, Monitoring, and Optimization. Chem. Rev 2010, 110, 2795; [PubMed: 20353192] (b)Ethirajan M; Chen Y; Joshi P; Pandey RK The Role of Porphyrin Chemistry in Tumor Imaging and Photodynamic Therapy. Chem. Soc. Rev 2011, 40, 340; [PubMed: 20694259] (c)Miao X; Hu W; He T; Tao H; Wang Q; Chen R; Jin L; Zhao H; Lu X; Fan Q; Huang W Deciphering the Intersystem Crossing in Near-Infrared BODIPY Photosensitizers for Highly Efficient Photodynamic Therapy. Chem. Sci 2019, 10, 3096; [PubMed: 30996892] (d)Chatteijee DK; Fong LS; Zhang Y Nanoparticles in Photodynamic Therapy: An Emerging Paradigm. Adv. Drug Delivery Rev 2008, 60, 1627;(e)Yano S; Hirohara S; Obata M; Hagiya Y; Ogura S.-i.; Ikeda A; Kataoka H; Tanaka M; Joh T Current States and Future Views in Photodynamic Therapy. J. Photochem. Photobiol. C: Photochem. Rev 2011, 12, 46;(f)O'Connor AE; Gallagher WM; Byrne AT Porphyrin and Nonporphyrin Photosensitizers in Oncology: Preclinical and Clinical Advances in Photodynamic Therapy. Photochem. Photobiol 2009, 85, 1053; [PubMed: 19682322] (g)Gai S; Yang G; Yang P; He F; Lin J; Jin D; Xing B Recent Advances in Functional Nanomaterials for Light-Triggered Cancer Therapy. Nano Today 2018, 19, 146;(h)Luo J; Chen L-F; Hu P; Chen Z-N Tetranuclear Gadolinium(III) Porphyrin Complex as a Theranostic Agent for Multimodal Imaging and Photodynamic Therapy. Inorg. Chem 2014, 53, 4184; [PubMed: 24693998] (i)Wang L; Yin H; Jabed MA; Hetu M; Wang C; Monro S; Zhu X; Kilina S; McFarland SA; Sun W π-Expansive Heteroleptic Ruthenium(II) Complexes as Reverse Saturable Absorbers and Photosensitizers for Photodynamic Therapy. Inorg. Chem 2017, 56, 3245; [PubMed: 28263079] (j)Yin H; Stephenson M; Gibson J; Sampson E; Shi G; Sainuddin T; Monro S; McFarland SA In Vitro Multiwavelength PDT with ^{3}IL States: Teaching Old Molecules New Tricks. Inorg. Chem 2014, 53, 4548; [PubMed: 24725142] (k)Donzello MP; Viola E; Ercolani C; Fu Z; Futur D; Kadish KM Tetra-2,3-pyrazinoporphyrazines with Externally Appended Pyridine Rings. 12. New Heteropentanuclear Complexes Carrying Four Exocyclic Cis-platin-like Functionalities as Potential Bimodal (PDT/Cis-platin) Anticancer Agents. Inorg. Chem 2012, 51, 12548. [PubMed: 23121685]

(7). (a)Dolmans DEJGJ; Fukumura D; Jain RK Photodynamic Therapy for Cancer. Nat. Rev. Cancer 2003, 3, 380; [PubMed: 12724736] (b)Lucky SS; Soo KC; Zhang Y Nanoparticles in Photodynamic Therapy. Chem. Rev 2015, 115, 1990; [PubMed: 25602130] (c)Lv Z; Wei H; Li Q; Su X; Liu S; Zhang KY; Lv W; Zhao Q; Li X; Huang W Achieving Efficient Photodynamic Therapy under Both Normoxia and Hypoxia using Cyclometalated Ru(II) Photosensitizer through Type I Photochemical Process. Chem. Sci 2018, 9, 502; [PubMed: 29619206] (d)Brian CW; Michael SP The Physics, Biophysics and Technology of Photodynamic Therapy. Phys. Med. Biol 2008, 53, R61. [PubMed: 18401068]

(8). (a)Lu K; He C; Lin W Nanoscale Metal–Organic Framework for Highly Effective Photodynamic Therapy of Resistant Head and Neck Cancer. J. Am. Chem. Soc 2014, 136, 16712; [PubMed: 25407895] (b)Lu K; He C; Lin W A Chlorin-Based Nanoscale Metal–Organic Framework for Photodynamic Therapy of Colon Cancers. J. Am. Chem. Soc 2015, 137, 7600; [PubMed: 26068094] (c)Zhang W; Lu J; Gao X; Li P; Zhang W; Ma Y; Wang H; Tang B Enhanced Photodynamic Therapy by Reduced Levels of Intracellular Glutathione Obtained By Employing a Nano-MOF with Cu^{II} as the Active Center. Angew. Chem. Int. Ed 2018, 57, 4891;(d)Ma Y; Li X; Li A; Yang P; Zhang C; Tang B H_2S-Activable MOF Nanoparticle Photosensitizer for Effective Photodynamic Therapy against Cancer with Controllable Singlet-Oxygen Release. Angew. Chem. Int. Ed 2017, 56, 13752;(e)Liu K; Xing R; Zou Q; Ma G; Möhwald H; Yan X Simple Peptide-Tuned Self-Assembly of Photosensitizers Towards Anticancer Photodynamic Therapy. Angew. Chem. Int. Ed 2016, 55, 3036;(f)Zou Q; Abbas M; Zhao L; Li S; Shen G; Yan X Biological Photothermal Nanodots Based on Self-Assembly of Peptide–Porphyrin Conjugates for Antitumor Therapy. J. Am. Chem. Soc 2017, 139, 1921; [PubMed: 28103663] (g)Naik A; Rubbiani R; Gasser G; Spingler B Visible-Light-Induced Annihilation of Tumor Cells with Platinum-Porphyrin Conjugates. Angew. Chem. Int. Ed 2014, 53, 6938;(h)Yu G; Yu S; Saha ML;

Zhou J; Cook TR; Yung BC; Chen J; Mao Z; Zhang F; Zhou Z; Liu Y; Shao L; Wang S; Gao C; Huang F; Stang PJ; Chen X A Discrete Organoplatinum(II) Metallacage as a Multimodality Theranostic Platform for Cancer Photochemotherapy. Nat. Commun 2018, 9, 4335; [PubMed: 30337535] (i)He Z; Dai Y; Li X; Guo D; Liu Y; Huang X; Jiang J; Wang S; Zhu G; Zhang F; Lin L; Zhu J-J; Yu G; Chen X Hybrid Nanomedicine Fabricated from Photosensitizer-Terminated Metal-Organic Framework Nanoparticles for Photodynamic Therapy and Hypoxia-Activated Cascade Chemotherapy. Small 2018, e1804131; [PubMed: 30565431] (j)Hisamatsu Y; Umezawa N; Yagi H; Kato K; Higuchi T Design and Synthesis of a 4-aminoquinoline-Based Molecular Tweezer that Recognizes Protoporphyrin IX and Iron(III) Protoporphyrin IX and its Application as a Supramolecular Photosensitizer. Chem. Sci 2018, 9, 7455; [PubMed: 30319746] (k)Monnereau C; Gomez J; Blart E; Odobel F; Wallin S; Fallberg A; Hammarström L Photoinduced Electron Transfer in Platinum(II) Terpyridinyl Acetylide Complexes Connected to a Porphyrin Unit. Inorg. Chem 2005, 44, 4806; [PubMed: 15962989] (l)Göransson E; Boixel J; Monnereau C; Blart E; Pellegrin Y; Becker H-C; Hammarström L; Odobel F Photoinduced Electron Transfer in Zn(II)porphyrin-Bridge-Pt(II)acetylide Complexes: Variation in Rate with Anchoring Group and Position of the Bridge. Inorg. Chem 2010, 49, 9823. [PubMed: 20919727]

(9). (a)Bechet D; Couleaud P; Frochot C; Viriot M-L; Guillemin F; Barberi-Heyob M Nanoparticles as Vehicles for Delivery of Photodynamic Therapy Agents. Trends Biotechnol. 2008, 26, 612; [PubMed: 18804298] (b)Lim C-K; Heo J; Shin S; Jeong K; Seo YH; Jang W-D; Park CR; Park SY; Kim S; Kwon IC Nanophotosensitizers Toward Advanced Photodynamic Therapy of Cancer. Cancer Lett. 2013, 334, 176; [PubMed: 23017942] (c)Liu K; Liu Y; Yao Y; Yuan H; Wang S; Wang Z; Zhang X Supramolecular Photosensitizers with Enhanced Antibacterial Efficiency. Angew. Chem. Int. Ed 2013, 52, 8285.

(10). (a)Schmitt F; Barry NPE; Juillerat-Jeanneret L; Therrien B Efficient Photodynamic Therapy of Cancer Using Chemotherapeutic Porphyrin–Ruthenium Metalla-Cubes. Bioorg. Med. Chem. Lett 2012, 22, 178. [PubMed: 22153934] (b)Schmitt F; Freudenreich J; Barry NPE; Juillerat-Jeanneret L; Süss-Fink G; Therrien B Organometallic Cages as Vehicles for Intracellular Release of Photosensitizers. J. Am. Chem. Soc 2012, 134, 754. [PubMed: 22185627] (c)Schmitt F; Govindaswamy P; Süss-Fink G; Ang WH; Dyson PJ; Juillerat-Jeanneret L; Therrien B Ruthenium Porphyrin Compounds for Photodynamic Therapy of Cancer. J. Med. Chem 2008, 51, 1811. [PubMed: 18298056] (d)Pernot M; Bastogne T; Barry NPE; Therrien B; Koellensperger G; Hann S; Reshetov V; Barberi-Heyob M Systems Biology Approach for in Vivo Photodynamic Therapy Optimization of Ruthenium-Porphyrin Compounds. J. Photoch. Photobio. B, Biol 2012, 117, 80.

(11). (a)He L; Liu Y; Lau J; Fan W; Li Q; Zhang C; Huang P; Chen X Recent Progress in Nanoscale Metal-Organic Frameworks for Drug Release and Cancer Therapy. Nanomedicine 2019, 14, 1343. [PubMed: 31084393] (b)Xiao Q; Zheng X; Bu W; Ge W; Zhang S; Chen F; et al. A Core/Satellite Multifunctional Nanotheranostic for in Vivo Imaging and Tumor Eradication by Radiation/Photothermal Synergistic Therapy. J. Am. Chem. Soc 2013, 135, 13041. [PubMed: 23924214] (c)Liu W; Liu T; Zou M; Yu W; Li C; He Z; Zhang M; Liu M; Li Z; Feng J; Zhang X Aggressive Man-Made Red Blood Cells for Hypoxia-Resistant Photodynamic Therapy. Adv. Mater, 2018, 30, 1802006.

(12). Rajora MA; Lou JWH; Zheng G Advancing Porphyrin's Biomedical Utility via Supramolecular Chemistry Chem. Soc. Rev 2017, 46, 6433. [PubMed: 29048439]

(13). (a)Prabhakar U; Maeda H; Jain RK; Sevick-Muraca EM; Zamboni W; Farokhzad OC; Barry ST; Gabizon A; Grodzinski P; Blakey DC Challenges and Key Considerations of the Enhanced Permeability and Retention Effect for Nanomedicine Drug Delivery in Oncology. Cancer Res. 2013, 73, 2412; [PubMed: 23423979] (b)Perez-Herrero E; Fernandez-Medarde, Advanced Targeted Therapies in Cancer: Drug Nanocarriers, the Future of Chemotherapy. A. Eur. J. Pharm. Biopharm 2015, 93, 52; [PubMed: 25813885] (c)Schottler S; Becker G; Winzen S; Steinbach T; Mohr K; Landfester K; Mailander V; Wurm FR Protein Adsorption is Required for Stealth Effect of Poly(ethylene glycol)- and Poly(phosphoester)-coated Nanocarriers. Nat. Nanotech 2016, 11, 372;(d)Kamaly N; Xiao Z; Valencia PM; Radovic-Moreno AF; Farokhzad OC Targeted Polymeric Therapeutic Nanoparticles: Design, Development and Clinical Translation. Chem. Soc. Rev 2012, 41, 2971. [PubMed: 22388185]

(14). (a)Thumshirn G; Hersel U; Goodman SL; Kessler H Multimeric Cyclic RGD Peptides as Potential Tools for Tumor Targeting: Solid-phase Peptide Synthesis and Chemoselective Oxime Ligation. Chem.-Eur. J 2003, 9, 2717; [PubMed: 12772286] (b)Iyer AK; Khaled G; Fang J; Maeda H Exploiting the Enhanced Permeability and Retention Effect for Tumor Targeting. Drug Discov. Today 2006, 11, 812; [PubMed: 16935749] (c)Miura Y; Takenaka T; Toh K; Wu S; Nishihara H; Kano MR; Ino Y; Nomoto T; Matsumoto Y; Koyama H; Cabral H; Nishiyama N; Kataoka K Cyclic RGD-Linked Polymeric Micelles for Targeted Delivery of Platinum Anticancer Drugs to Glioblastoma through the Blood-Brain Tumor Barrier. ACS Nano 2013, 7, 8583. [PubMed: 24028526]

(15). (a)Jana A; McKenzie L; Wragg AB; Ishida M; Hill JP; Weinstein JA; Baggaley E; Ward MD Porphyrin/Platinum(II) CNN Acetylide Complexes: Synthesis, Photophysical Properties, and Singlet Oxygen Generation. Chem.-Eur. J 2016, 22, 4164; [PubMed: 26849274] (b)Guo Z; Zou Y; He H; Rao J; Ji S; Cui X; Ke H; Deng Y; Yang H; Chen C; Zhao Y; Chen H Bifunctional Platinated Nanoparticles for Photoinduced Tumor Ablation. Adv. Mater 2016, 28, 10155. [PubMed: 27714878]

(16). Schottelius M; Laufer B; Kessler H; Wester H-J Ligands for Mapping $\alpha_v\beta_3$-Integrin Expression in Vivo. Acc. Chem. Res 2009, 42, 969. [PubMed: 19489579]

(17). Woods JA; Ferguson JS; Kalra S; Degabriele A; Gardner J; Logan P; Ferguson J The phototoxicity of vemurafenib: An investigation of clinical monochromator phototesting and in vitro phototoxicity testing. Journal of Photochemistry and Photobiology B: Biology 2015, 151, 233.

(18). (a)Knop K; Hoogenboom R; Fischer D; Schubert US Poly(ethylene glycol) in Drug Delivery: Pros and Cons as Well as Potential Alternatives. Angew. Chem. Int. Ed 2010, 49, 6288;(b)Liu XS; Li H; Chen YJ; Jin Q; Ren KF; Ji J Mixed-Charge Nanoparticles for Long Circulation, Low Reticuloendothelial System Clearance, and High Tumor Accumulation. Adv. Healthc. Mater 2014, 3, 1439. [PubMed: 24550205]

(19). Yang H-B; Das N; Huang F; Hawkridge AM; Muddiman DC; Stang PJ Molecular Architecture via Coordination: Self-Assembly of Nanoscale Hexagonal Metallodendrimers with Designed Building Blocks. J. Am. Chem. Soc 2006, 128, 10014. [PubMed: 16881621]

(20). Berezina NM; Bazanov MI; Semeikin AS; Glazunov AV Electrochemical and Electrocatalytic Properties of Tetra(pyridyl-4′,3′)porphin Series Derivatives. Russ. J. Electrochem 2011, 47, 42.

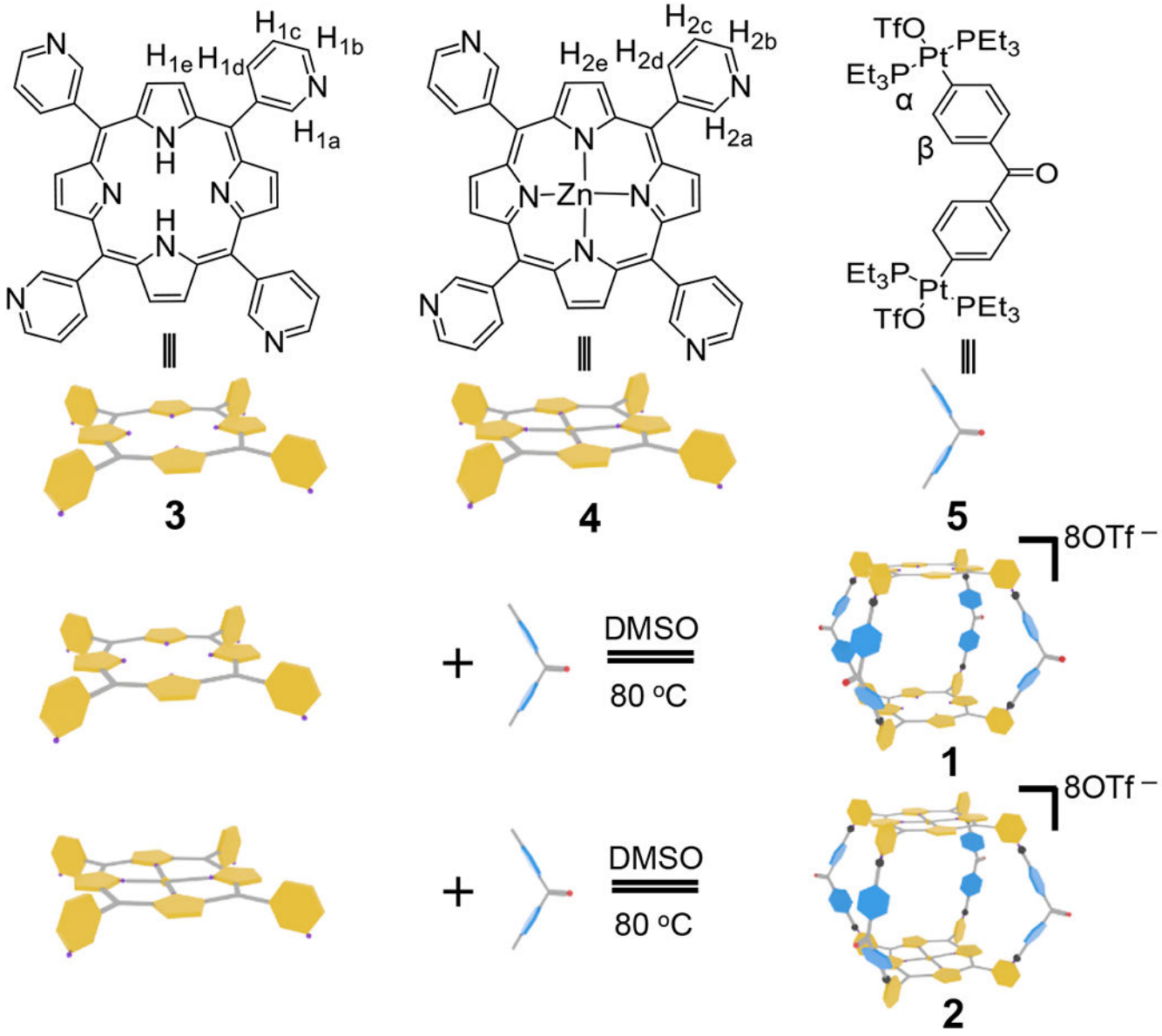

Figure 1.
Self-assembly of supramolecular cages **1** and **2**.

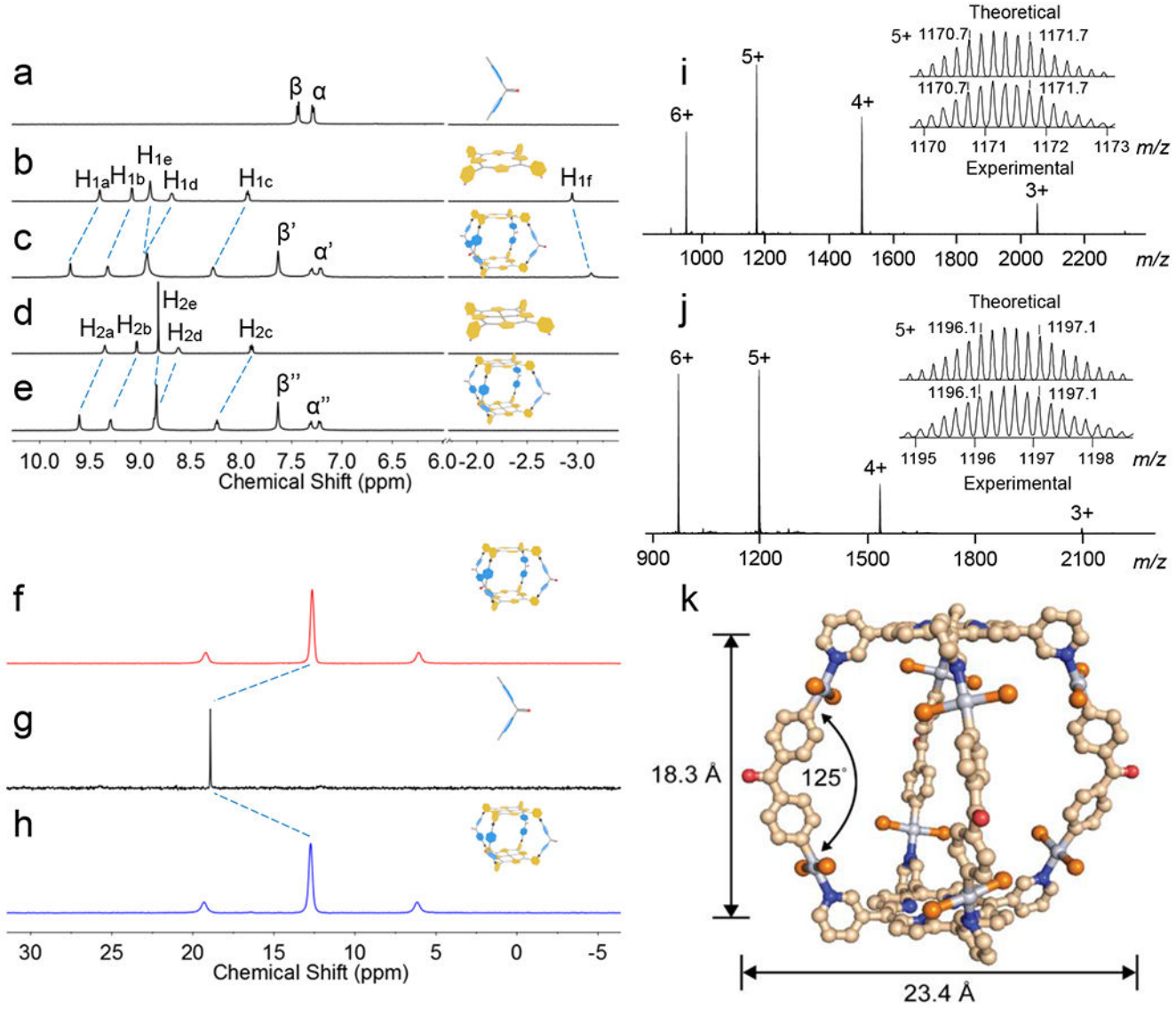

Figure 2.

The structural characterization of metallacages. Partial ^{1}H NMR (a–e) and ^{31}P{^{1}H} (f–h) spectra (500 MHz, DMSO-d_6, 300 K) of **5** (a , g), **3** (b), **1** (c and f), **4** (d) and **2** (e, h). ESI-MS spectra of complexes **1** (i) and **2** (j). X-ray crystal structure of **1** (k).OTf anions and the ethyl groups on PEt_3 are omitted for the sake of clarity.

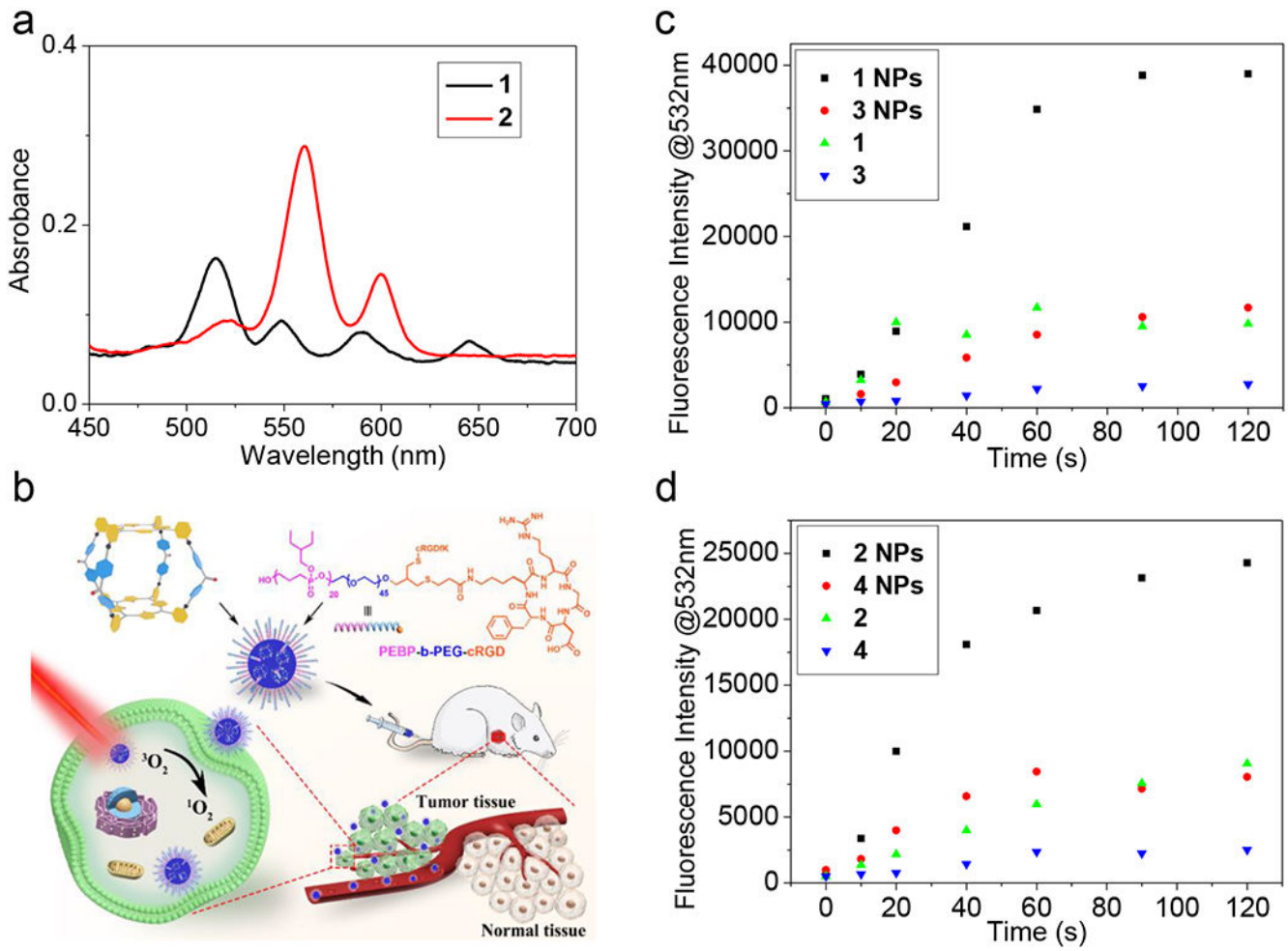

Figure 3.

Photophysical research and cartoon representation of PDT. (a) UV-Vis absorption spectra of 1 and 2 in DMSO (c= 1×10^{-5} M, 298K). (b) Schematic diagrams of the **1 NPs** for cancer treatment. (c, d) Fluorescence intensity of the solution containing SOSG and different nanoparticles at 532 nm as a function of irradiation time (638 nm, 0.5 W/cm^2).

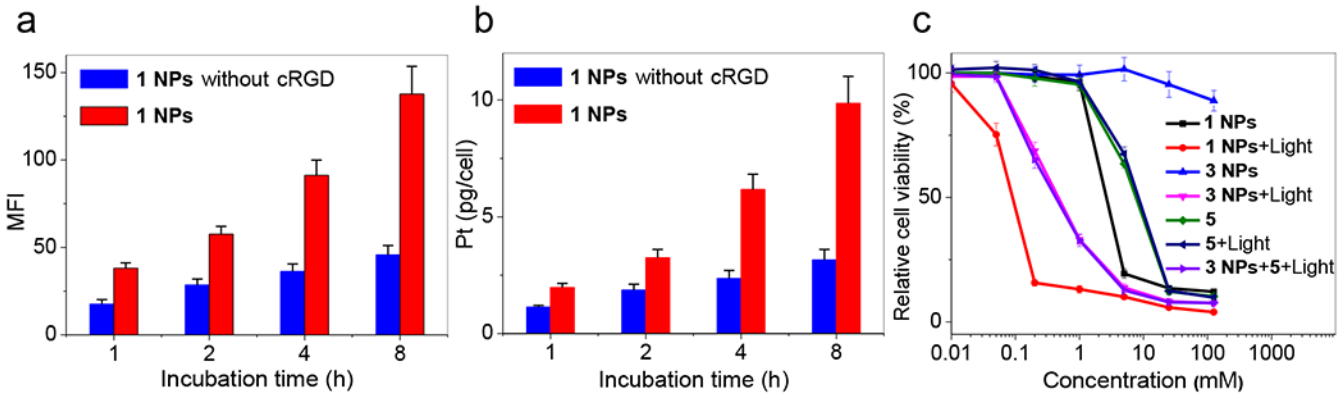

Figure 4.

In vitro cell uptake and cytotoxicity of **1 NPs**. (a) Mean fluorescent intensity (MFI) and intracellular platinum amount of 4T1 cells after treatment with the **1 NPs** with or without cRGD targeting moiety for different incubation times (b). (c) Relative cell viability of 4T1 cells treated with different administrations.

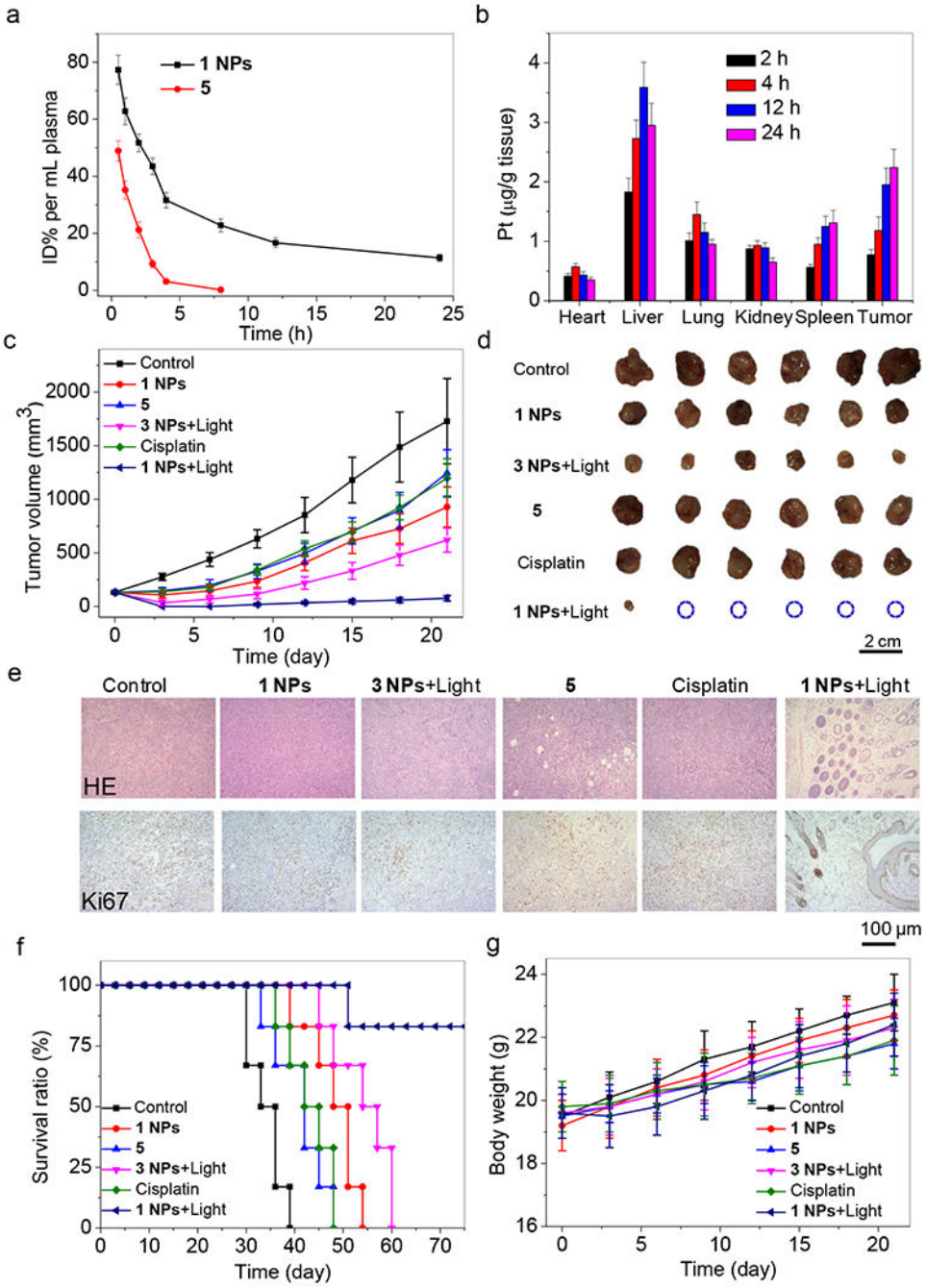

Figure 5.

In vivo distribution and anti-tumor effect on 4T1 orthotopic breast cancer-bearing mice. (a) *In vivo* blood elimination kinetics of **5** and the **1 NPs** at a dose of 2 mg Pt/kg body weight (n = 4). (b) Tissue distributions of the platinum in the main organs after i.v. injection of the **1 NPs** at a dose of 2 mg Pt/kg body weight (n = 4) for different times. (c) Tumor volume as a function of time after different treatments (n = 6). (d) Photos of 4T1 orthotopic tumors harvested from the mice receiving different treatments. (e) H&E and Ki67 analyses of tumor tissues after various treatments. Ki67-positive tumor cells were stained brown. Scale bar is

100 μm. (f) Kaplan-Meier plots and (g) body weights of the mice bearing 4T1 tumors after different treatments. The irradiation density was 0.5 W/cm^2 at 638 nm for 6 min. Data are expressed as means ± s.e.m., **P<0.01.